

See discussions, stats, and author profiles for this publication at: <https://www.researchgate.net/publication/266376279>

Electrical, Chemical, and Electrochemical Properties of Double Perovskite Oxides $\text{Sr}_2\text{Mg}_{1-x}\text{Ni}_x\text{Mo}_6-\delta$ as Anode Materials for Solid Oxide Fuel Cells

ARTICLE *in* THE JOURNAL OF PHYSICAL CHEMISTRY C · JULY 2014

Impact Factor: 4.77 · DOI: 10.1021/jp502503e

CITATIONS

2

READS

58

5 AUTHORS, INCLUDING:



Hailei Zhao

University of Science and Technology Beijing

169 PUBLICATIONS 1,957 CITATIONS

[SEE PROFILE](#)



Zhihong Du

University of Science and Technology Beijing

22 PUBLICATIONS 78 CITATIONS

[SEE PROFILE](#)

Electrical, Chemical, and Electrochemical Properties of Double Perovskite Oxides $\text{Sr}_2\text{Mg}_{1-x}\text{Ni}_x\text{MoO}_{6-\delta}$ as Anode Materials for Solid Oxide Fuel Cells

Zhixiang Xie,[†] Hailei Zhao,^{*,†,‡} Zhihong Du,[†] Ting Chen,[†] and Ning Chen^{†,‡}

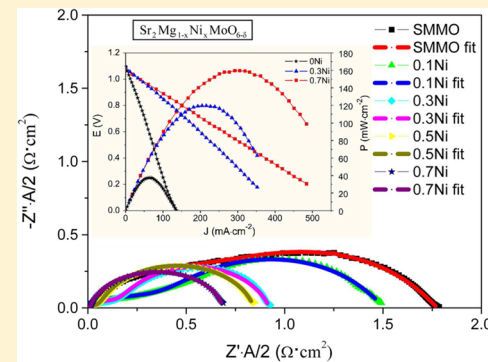
[†]School of Materials Science and Engineering, University of Science and Technology Beijing, Beijing 100083, China

[‡]Beijing Key Laboratory of New Energy Materials and Technologies, Beijing 100083, China

ABSTRACT: The suitability of double perovskite oxides of composition $\text{Sr}_2\text{Mg}_{1-x}\text{Ni}_x\text{MoO}_{6-\delta}$ (SMNM, $x = 0$ –0.9) as anode materials for solid oxide fuel cells (SOFCs) was evaluated. Single double perovskite structures could be obtained up to $x = 0.9$ in syntheses at ambient atmosphere. However, after reduction at 800 °C, trace amounts of impurities were detected in the sample with $x = 0.9$, suggesting that the upper limit for the Ni content (x) in SMNM is less than 0.9 under SOFC operating conditions. The electrical conductivity of SMNM increases with increasing Ni content because of the increase in the concentration of electronic defects, $[\text{Mo}^{5+}_{\text{Mo}^{6+}}]$, and the decreased band gap energy, as revealed by first-principles calculations. The substitution of Ni can facilitate the charge-transfer process of the electrode reaction, decrease the polarization resistance, and thus increase the power density of a single cell. X-ray photoelectron spectroscopy and temperature-programmed reduction measurements were used to explain the reason for the performance improvement. SMNM showed good chemical compatibility with $\text{Ce}_{0.8}\text{Sm}_{0.2}\text{O}_{2-\delta}$ (SDC) but a slight reactivity with the electrolyte $\text{La}_{0.8}\text{Sr}_{0.2}\text{Ga}_{0.83}\text{Mg}_{0.17}\text{O}_{3-\delta}$ (LSGM) at 1300 °C. The use of an SDC buffer layer could avoid the interface reaction between the SMNM anode and the LSGM electrolyte, resulting in better cell performance. The $\text{Sr}_2\text{Mg}_{0.3}\text{Ni}_{0.7}\text{MoO}_{6-\delta}$ electrode exhibited a maximal power density of 160 mW cm⁻² at 800 °C with an electrolyte (LSGM, 400 μm)-supported cell configuration.

1. INTRODUCTION

Solid oxide fuel cells (SOFCs) are all-solid electrochemical reactors that convert chemical energy directly into electricity by means of the chemical reaction between hydrogen and oxygen to produce water.¹ Because of the high energy conversion efficiency, absence of noise, and low chemical pollution, SOFCs are regarded as a promising electricity generation technology in the future. However, the commercialization of SOFCs faces many challenges. Direct utilization of more available fuels such as hydrocarbons to replace H₂ is the key issue to accelerate the practical application of SOFCs.² Ni-YSZ cermet is the traditional anode material, which exhibits excellent performance when using H₂ as fuel but shows a decline in performance when operating with natural gas because it promotes carbon deposition and sulfur poisoning,^{3,4} which deteriorate the catalytic activity of Ni and, as a result, progressively increase the electrode polarization. To solve these problems, many research efforts have been devoted to the development of external/internal steam reforming before the hydrocarbon gas is conducted into the anode chamber. However, this strategy increases the cost of investment or decreases the fuel availability and the power density of the cells. Therefore, exploring new anode materials that are suitable for working with hydrocarbon fuels directly is one of the main targets for the development of SOFCs.



A viable anode material should have appropriate electronic and ionic conductivities over a wide range of oxygen partial pressures, high electrocatalytic activity toward fuel oxidation, and good chemical stability and thermal compatibility with the electrolyte and interconnecting materials under SOFC operating conditions.⁵ Different structure types, such as fluorite-type ($\text{Gd}_{0.1}\text{Ce}_{0.9}\text{O}_{1.95}$), perovskite-type ($\text{La}_{0.75}\text{Sr}_{0.25}\text{Cr}_{0.5}\text{Mn}_{0.5}\text{O}_{3-\delta}$ and $\text{Sr}_{0.86}\text{Y}_{0.08}\text{TiO}_{3-\delta}$), pyrochlore-type ($\text{Gd}_2\text{TiMoO}_{7\pm\delta}$), and tungsten-bronze-type ($\text{Sr}_{0.2}\text{Ba}_{0.4}\text{Ti}_{0.2}\text{Nb}_{0.8}\text{O}_3$) materials, have been investigated as potential anode materials.^{6–11} Recently, the double perovskite $\text{Sr}_2\text{MgMoO}_{6-\delta}$ (SMMO) was proposed as an anode material for SOFCs because of its mixed ionic-electronic conducting feature and good electrocatalytic activity toward fuel oxidation. Besides, SMMO has appreciable stability in a variety of fuels and presents strong resistance to carbon deposition and sulfur poisoning. The power density of cells with SMMO anodes can reach 840 mW cm⁻² in H₂ at 800 °C, while the anode can resist 50 ppm H₂S in H₂ with negligible performance loss.^{12–14} However, some work revealed that SMMO actually has poor electrocatalytic activity, and the good anode performance was obtained only by using Pt paste as a current collector.¹⁵

Received: March 12, 2014

Revised: July 29, 2014

Published: July 30, 2014

Additionally, the low electrical conductivity is another problem for SMMO, which easily causes electrode polarization and hence affects the power density of the cells.

The double perovskite oxide SMMO has a B-site ordered structure, differing from the simple perovskite, because the B-site sublattice is occupied by two different cations (Mg and Mo) that are different enough from each other both in charge and ionic radius. This structural characteristic provides many positions for doping to improve various properties, such as electrical conductivity, electrocatalytic activity, and chemical stability. Partial substitution of La³⁺, Sm³⁺, and Ba²⁺ for Sr in Sr₂MgMoO_{6-δ} can improve the electrical conductivity¹⁶ and electrocatalytic properties for hydrocarbon oxidation¹⁷ but deteriorates the structural stability under oxidizing conditions.^{18,19} All of the substitutions of Mn, Fe, and Cr for Mg enhance the electrical conductivity, but the resulting products are much more sensitive to oxygen partial pressure (P_{O_2}), that is, the electrical conductivity decreases sharply with increasing P_{O_2} .^{13,18} Substitution of W and Nb for Mo in SMMO slightly decreases the electrical conductivity, while an appropriate amount of Nb can increase the concentration of oxygen vacancies,^{20,21} which contribute much to the electrode performance. In order to produce enough oxygen vacancies in SMMO, Huang et al.^{13,14} reduced the sample in 5% H₂/Ar at 800 °C for 20 h before cell measurement. Marrero-López et al.,¹⁸ Bernuy-Lopez et al.,²² and Matsuda et al.²³ indicated that the concentration of oxygen vacancies in SMMO is very limited even under strongly reducing conditions. Our previous work revealed that doping of Co on the Mg site of SMMO can simultaneously improve the electronic and ionic conductivities as well as the electrochemical performance.²⁴ However, the Co-doped SMMO presents poor structural stability under a reducing atmosphere. Huang et al.^{25,26} reported that Sr₂NiMoO₆ has better structural stability than Sr₂CoMoO₆ because of the stronger Ni–O octahedra compared with Co–O octahedra.

In the present study, Ni was selected as the Mg-site dopant to prepare double perovskites Sr₂Mg_{1-x}Ni_xMoO_{6-δ} (SMNM). Taking the advantage of high redox ability of Ni, the partial substitution of Ni for Mg can increase the conduction channels of small polaron jumping along B–O–B bonds, decrease the conduction activation energy, and thus enhance the electronic conductivity of the material. Meanwhile, Ni doping has the potential to improve the electrocatalytic activity of the electrode. Because of the weaker Ni–O bond compared with Mg–O, Ni doping can give rise to the generation of more oxygen vacancies, which are desirable for a better anode reaction. We systematically characterized the effects of Ni substitution on the structure and properties of SMNM as an anode material for SOFCs in terms of crystal structure, electrical conductivity, chemical compatibility with the electrolyte, and electrochemical performance. The electronic conduction mechanism is discussed on the basis of first-principles calculations and X-ray photoelectron spectroscopy (XPS) examination.

2. EXPERIMENTAL SECTION

The double perovskites Sr₂Mg_{1-x}Ni_xMoO_{6-δ} ($x = 0\text{--}0.9$) were prepared by using a nitrate–citrate combustion method. Briefly, stoichiometric amounts of Sr(NO₃)₂, Mg(NO₃)₂·6H₂O, Ni(NO₃)₂·6H₂O, and (NH₄)₆Mo₇O₂₄·4H₂O (all A.R. grade) were dissolved in deionized water, and then citric acid monohydrate

was introduced as the chelating agent at a total metal ion:citric acid monohydrate molar ratio of 1:2. The obtained solution was agitated with a magnetic stirring apparatus for 2 h and then kept in an 80 °C water bath until a perfect gel was formed. This gel was slowly heated in an oven until combustion occurred. The resultant black powder was then ground and calcined in air at 800 °C for 10 h to remove the organic component. The product was ground again and uniaxially pressed into bars (42 mm × 8 mm × 3 mm) and pellets (diameter = 19 mm), which were sintered at 1450 °C for 10 h in air (denoted as sintered samples) and then reduced at 800 °C for 24 h in 5% H₂/Ar (denoted as reduced samples) to get relative densities higher than 90% for bulk density and electrical conductivity measurements. In order to prevent the volatilization of MoO₃ during high-temperature synthesis, MoO₃ powder was placed beside the sample to build MoO₃ vapor pressure. The density of the sintered pellets was measured by the Archimedes method. Powders of the La_{0.8}Sr_{0.2}Ga_{0.8}Mg_{0.2}O_{3-δ} (LSGM) electrolyte were also prepared by the citric acid–nitrate method.²⁷

X-ray diffraction (XRD) on a Rigaku D/max-A X-ray diffractometer with Cu K α radiation was used to identify the phase and crystal structure of each sample. Microstructures of the sintered pellets were observed with a LEO-1450 scanning electron microscope (SEM). The valence states of Mo and O were determined by XPS on a RBD upgraded PHI-5000C ESCA system (PerkinElmer) with Mg K α radiation. The charge referencing was performed against the binding energy of adventitious carbon (C 1s = 284.6 eV). Temperature-programmed reduction (TPR) was employed to examine the lattice oxygen release of each sample with increasing temperature, which was performed in a U-shaped quartz microreactor at a heating rate of 5 °C min⁻¹ in 5% H₂/Ar flowing at a rate of 30 mL min⁻¹.

The chemical compatibility of SMNM with LSGM and Sm_{0.2}Ce_{0.8}O_{2-δ} (SDC) electrolytes was examined. The Sr₂Mg_{0.3}Ni_{0.7}MoO_{6-δ} powder with pure double perovskite structure prepared at 1250 °C was mixed with LSGM or SDC electrolyte powder in a weight ratio of 1:1 to get SMNM/electrolyte mixtures, which were pressed and calcined at 1300 °C for 10 h in air. The calcined pellets were crushed and examined by XRD to investigate the phase changes after the heat treatment.

The electrical conductivities of all samples were measured by a standard four-terminal DC method²⁸ in 5% H₂/Ar from 100 to 900 °C. Symmetrical cells of SMNM/LSGM/SMNM were used for impedance measurements over the temperature range of 700–850 °C with a Solartron 1260 frequency response analyzer in combination with a Solartron 1287 potentiostat over the frequency range of 10⁻² to 10⁶ Hz with an AC signal amplitude of 5 mV. The dense LSGM electrolyte with a thickness of 400 μm used for the fabrication of symmetrical cells was prepared by sintering the pellet in air at 1450 °C for 6 h. The electrode slurry was prepared by mixing SMNM powder with α-terpineol and ethyl cellulose using starch as a pore former. The symmetric cells were fabricated by symmetrically screen-printing the electrode slurry on both surfaces of the LSGM disk followed by a heat treatment at 1300 °C for 2 h.

Single fuel cells were fabricated in a electrolyte-supporting configuration with a 400 μm thick LSGM pellet as the electrolyte, SMNM as the anode and SmBaCo₂O_{5+δ} as the cathode. Electrode slurries were prepared by mixing the prepared SMNM and SmBaCo₂O_{5+δ} powders with α-terpineol and ethyl cellulose. The SMNM anode slurry was screen-

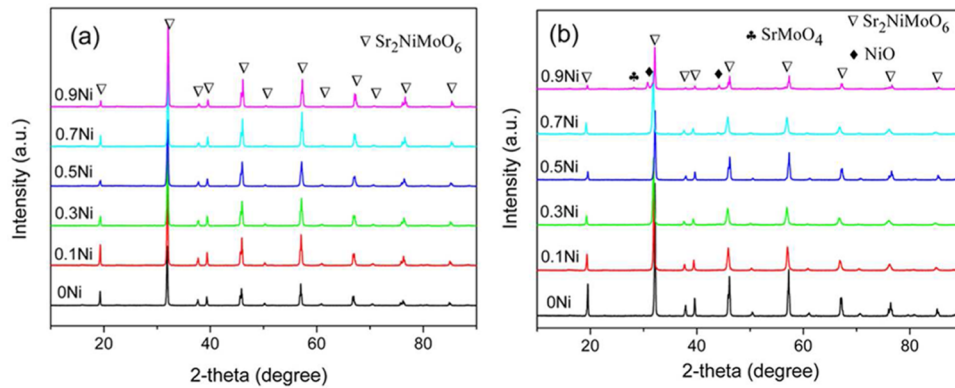


Figure 1. XRD patterns of $\text{Sr}_2\text{Mg}_{1-x}\text{Ni}_x\text{MoO}_{6-\delta}$ (a) after sintering in air at $1450\text{ }^\circ\text{C}$ for 10 h and (b) after sintering in air at $1450\text{ }^\circ\text{C}$ for 10 h followed by reduction in 5% H_2/Ar at $800\text{ }^\circ\text{C}$ for 24 h.

printed onto one side of the LSGM pellet and then heated at $1300\text{ }^\circ\text{C}$ for 2 h in air. Subsequently, the $\text{SmBaCo}_2\text{O}_{5+\delta}$ cathode slurry was screen-printed on the other side of the electrolyte and heated in air at $1000\text{ }^\circ\text{C}$ for 2 h. For some cells, in order to prevent the chemical reaction between SMNM and LSGM, a buffer layer of SDC was introduced between them by calcination at $1300\text{ }^\circ\text{C}$ in air for 1 h before anode preparation. After cell preparation, the electrode surfaces were covered with silver paste as a current collector and then calcined at $600\text{ }^\circ\text{C}$ for 30 min in air. The effective area of the electrodes was 0.453 cm^2 . A ceramic-based sealant (Ceramabond 552-VFG, Aremco) was used to seal the gas compartments of the single cell.

Before cell testing, the anode was exposed to pure H_2 for 4 h at $800\text{ }^\circ\text{C}$ to reduce the SMNM. Fuel cell measurements were performed at $800\text{ }^\circ\text{C}$ using humidified H_2 at a flow rate of 30 mL min^{-1} as the fuel and static air as the oxidant. The measurement was started after the open-circuit voltage remained unchanged. The potential–current density (E – J) data for the cell were recorded by holding at each temperature for at least 15 min until no significant changes were observed.

In the present study, the average binding energy of SMMO with and without Ni substitution for Mg was calculated using the CASTEP module of Materials Studio software (Accelrys) based on density functional theory (DFT). According to the total-energy plane-wave pseudopotential route, the particle potential was replaced with the pseudopotential and the electron wave function was expanded with a plane-wave basis set. The general Perdew–Burke–Ernzerhof (PBE) functional of the generalized gradient approximation (GGA) was employed for the exchange and correlation of electrons.²⁹ During the Broyden–Fletcher–Goldfarb–Shanno (BFGS) calculation, the cutoff energy of the plane-wave basis set and the convergence error of the total energy were 380 eV and $1.0 \times 10^{-5}\text{ eV atom}^{-1}$, respectively.

3. RESULTS AND DISCUSSION

3.1. Phase and Microstructure Development. Figure 1a shows the XRD patterns of the $\text{Sr}_2\text{Mg}_{1-x}\text{Ni}_x\text{MoO}_{6-\delta}$ ($x = 0$ – 0.9) samples sintered in air at $1450\text{ }^\circ\text{C}$ for 10 h. All of the peaks of the samples were indexed as single double-perovskite structures without any impurities. Since the SOFC anode is operated in the environment of low oxygen partial pressure, all of the samples were subjected to reduction at $800\text{ }^\circ\text{C}$ in 5% H_2/Ar for 24 h to examine their structural stability. As shown in Figure 1b, only when the doping amount of Ni (x) was no more than 0.9 could a pure double perovskite phase be

obtained for SMNM. Trace amounts of impurities of NiO and SrMoO_4 were detected in the sample with $x = 0.9$. The binding energy, which is the energy needed to dissociate the crystal into infinitely separated static neutral atoms, is an important factor influencing the structural stability of crystalline materials. First-principles calculations demonstrated that Ni-doped SMMO has a lower binding energy (14429 eV) than SMMO (14805 eV), which can partially account for the appearance of impurities in the sample with $x = 0.9$ under reducing conditions. Too much Ni doping is apparently detrimental to the structural stability of SMMO under a reducing atmosphere. Although Ji et al.¹⁷ reported that $\text{Sr}_2\text{NiMoO}_6$ was synthesized in 5% H_2/Ar at $1100\text{ }^\circ\text{C}$, Vasala et al.³⁰ found that pure $\text{Sr}_2\text{NiMoO}_6$ could not be synthesized under a reducing atmosphere, which is consistent with our results.

The structural stability of the $\text{Sr}_2\text{Mg}_{0.3}\text{Ni}_{0.7}\text{MoO}_{6-\delta}$ samples was further evaluated under pure H_2 . After heat treatment of the synthesized $\text{Sr}_2\text{Mg}_{0.3}\text{Ni}_{0.7}\text{MoO}_{6-\delta}$ powders in pure H_2 at $800\text{ }^\circ\text{C}$ for 5 h, only the double perovskite phase without any other impurity could be detected (Figure 2), indicating the good structural stability of the $\text{Sr}_2\text{Mg}_{1-x}\text{Ni}_x\text{MoO}_{6-\delta}$ ($x = 0$ – 0.7) anodes in the operating environment of SOFCs.

3.2. Electrical Conductivity of Ni-Doped SMMO. The total electrical conductivities (σ) of $\text{Sr}_2\text{Mg}_{1-x}\text{Ni}_x\text{MoO}_{6-\delta}$ ($x = 0$ – 0.7) reduced samples measured by the four-point DC method under reducing conditions (5% H_2/Ar) over the temperature range of 100 – $900\text{ }^\circ\text{C}$ are presented in Figure 3a.

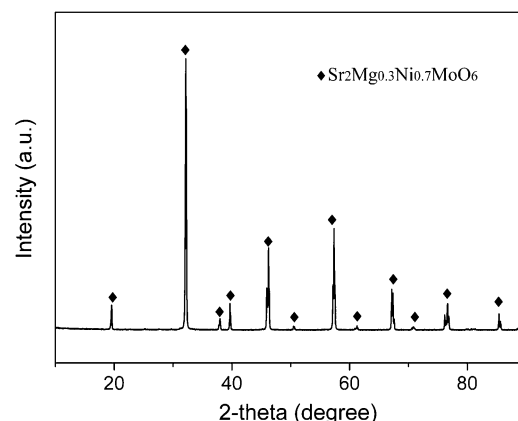


Figure 2. XRD pattern of $\text{Sr}_2\text{Mg}_{0.3}\text{Ni}_{0.7}\text{MoO}_{6-\delta}$ synthesized in air at $1450\text{ }^\circ\text{C}$ for 10 h and then reduced in H_2 at $800\text{ }^\circ\text{C}$ for 5 h.

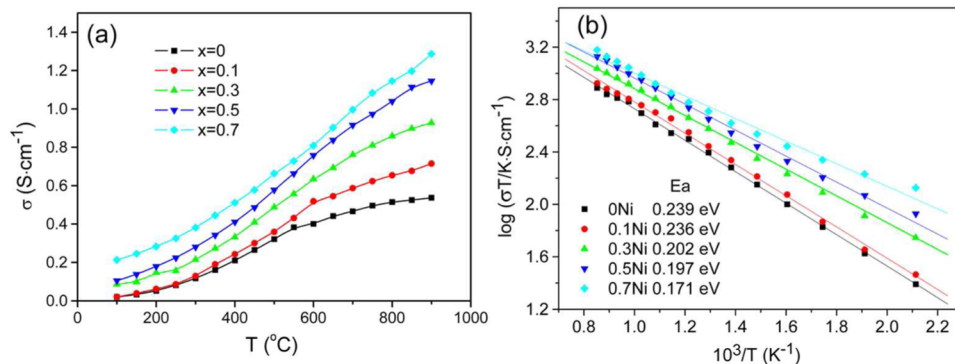


Figure 3. (a) Temperature dependence of the electrical conductivity of $\text{Sr}_2\text{Mg}_{1-x}\text{Ni}_x\text{MoO}_{6-\delta}$. (b) Arrhenius plots of the conductivity.

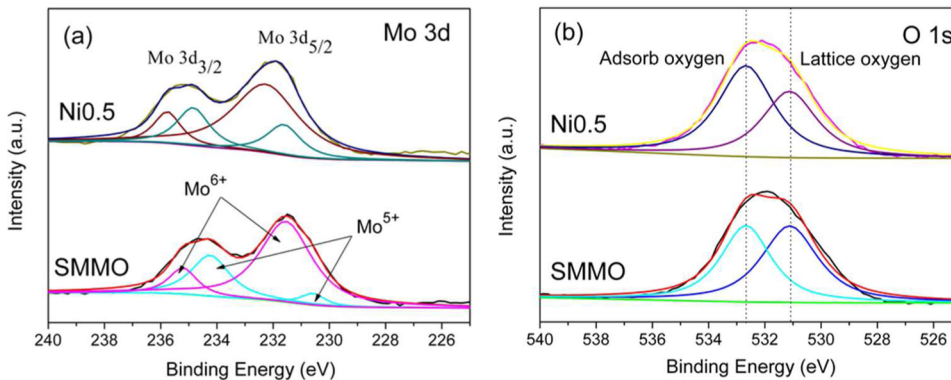


Figure 4. XPS spectra of SMMO and $\text{Sr}_2\text{Mg}_{0.5}\text{Ni}_{0.5}\text{MoO}_6$: (a) Mo 3d; (b) O 1s.

Table 1. Fitting Results for the Mo 3d XPS Spectra of SMMO and $\text{Sr}_2\text{Mg}_{0.5}\text{Ni}_{0.5}\text{MoO}_6$

sample	parameter	Mo ⁶⁺		Mo ⁵⁺		Mo ⁶⁺ /Mo ⁵⁺ ratio
		Mo 3d _{3/2}	Mo 3d _{5/2}	Mo 3d _{3/2}	Mo 3d _{5/2}	
SMMO	BE (eV)	231.8	235.2	230.6	234.2	2.65
	area	35824	6239	2423	13356	
0.5Ni	BE (eV)	232.2	235.9	231.8	234.9	2.35
	area	38430	7203	8898	10488	

The increase in temperature obviously results in a rapid increase in the conductivity. There is a linear relationship between $\ln(\sigma T)$ and $1/T$ in the corresponding Arrhenius plots (Figure 3b), suggesting a small polaron conduction behavior. The activation energies (E_a) for electron conduction for different samples could be derived from the slopes of the linear fits, and the values are listed in Figure 3b. The decreasing E_a of SMNM with Ni content indicates that Ni doping alters the electronic structure of the material and makes it much more favorable for electron conduction.

With an increase in Ni doping amount, the conductivity of SMNM increased obviously. Besides the activation energy, the charge carrier concentration is another factor that influences the electrical conductivity of a semiconductor. The oxidation state of Mo ions determines the charge carrier concentration in SMNM. To obtain a clear understanding of charge compensation in $\text{Sr}_2\text{Mg}_{1-x}\text{Ni}_x\text{MoO}_6$, XPS measurements were performed to identify the valence states of Mo ions in the Ni-doped and undoped samples. The Mo 3d XPS spectra of SMMO and $\text{Sr}_2\text{Mg}_{0.5}\text{Ni}_{0.5}\text{MoO}_{6-\delta}$ are presented in Figure 4a. The Mo 3d XPS spectra are split into two asymmetrical peaks assignable to 3d_{3/2} and 3d_{5/2}, whose binding energies are around 232 and 235 eV, respectively. The spectra were fit

(using the XPSpeak4.1 software) to two pairs of peaks that correspond to Mo⁶⁺ and Mo⁵⁺.³¹⁻³³ The detailed binding energies of the different peaks for the investigated samples are listed in Table 1. Although both samples exhibited Mo⁵⁺/Mo⁶⁺ mixed valence, the Ni-doped sample showed apparently higher Mo⁵⁺ content relative to the undoped SMMO, according to the ratio of the integrated areas of the Mo⁵⁺ and Mo⁶⁺ peaks. This result revealed that Ni substitution for Mg increases the charge carrier concentration, [Mo⁵⁺_{Mo⁶⁺}'], which is one of the reasons for the enhanced electronic conductivity. This is probably associated with the weaker Ni–O bond compared with the Mg–O bond, which would allow more lattice oxygen to be released under a reducing atmosphere at elevated temperature. As a result, more oxygen vacancies and free electrons would be produced. The free electrons would then be localized by Mo⁶⁺ ions to produce Mo⁵⁺ ions.

The XPS results for the O 1s components for SMMO and $\text{Sr}_2\text{Mg}_{0.5}\text{Ni}_{0.5}\text{MoO}_{6-\delta}$ are shown in Figure 4b. An asymmetrical peak was observed for both samples, which could be deconvoluted into two peaks. They corresponded to two different kinds of oxygen species: lattice oxygen and adsorbed oxygen. The $\text{Sr}_2\text{Mg}_{0.5}\text{Ni}_{0.5}\text{MoO}_{6-\delta}$ sample exhibited a higher adsorbed oxygen content than SMMO, suggesting that Ni

doping improves the catalytic activity toward the oxygen association/dissociation process.

In order to gain a better understanding of the Ni-doping effect on the electrical conduction behavior, first-principles calculations based on DFT were performed to get the energy band structures of samples SMMO and $\text{Sr}_2\text{Mg}_{0.5}\text{Ni}_{0.5}\text{MoO}_{6-\delta}$. The binding energies and electronic densities of states (DOS) were calculated using Materials Studio software with the supercell models shown in Figure 5a (SMMO) and Figure 5b

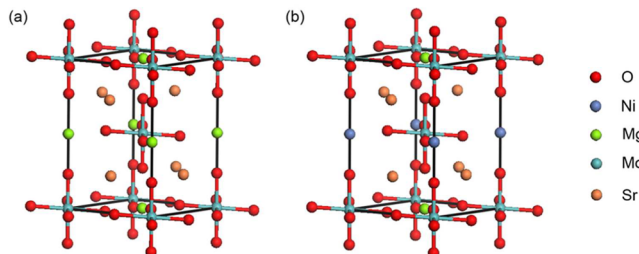
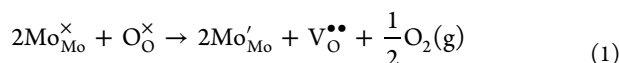


Figure 5. Lattice models for (a) SMMO and (b) $\text{Sr}_2\text{Mg}_{0.5}\text{Ni}_{0.5}\text{MoO}_{6-\delta}$.

($\text{Sr}_2\text{Mg}_{0.5}\text{Ni}_{0.5}\text{MoO}_{6-\delta}$). The results indicated that Ni doping decreases the binding energy of the SMNM crystal, which makes the release of lattice oxygen under reducing conditions much easier. From the viewpoint of defect chemistry, the loss of lattice oxygen could lead to the generation of oxygen vacancies as well as partial reduction of Mo^{6+} to Mo^{5+} to maintain the electroneutrality, as elucidated by eq 1, which is beneficial to both electronic and ionic conductivities. This result is consistent with the XPS finding shown in Figure 4.



The electronic DOS for SMMO and $\text{Sr}_2\text{Mg}_{0.5}\text{Ni}_{0.5}\text{MoO}_{6-\delta}$ as functions of energy are presented in Figure 6a,b, respectively. The Ni substitution has a great impact on the DOS of SMMO. A donor energy level is generated by Ni doping, causing the Fermi level to move nearer to the valence band. As a result, the band gap energy for electron conduction is decreased. Therefore, it is further confirmed that the increased electrical conductivity with increasing Ni content in $\text{Sr}_2\text{Mg}_{1-x}\text{Ni}_x\text{MoO}_{6-\delta}$ is ascribable to the increasing concentration of localized electrons and the decreasing activation energy of electron hopping.

3.3. Chemical Compatibility with Electrolytes. Chemical reactions at the interface between the electrolyte and the

anode may create an insulating phase, which would increase the polarization resistance of the electrode. In order to assess the chemical compatibility of Ni-doped SMMO with LSGM and SDC electrolytes, pellets composed of $\text{Sr}_2\text{Mg}_{0.3}\text{Ni}_{0.7}\text{MoO}_{6-\delta}$ and LSGM or $\text{Sr}_2\text{Mg}_{0.3}\text{Ni}_{0.7}\text{MoO}_{6-\delta}$ and SDC in a weight ratio of 1:1 were selected as representatives for heat treatment at 1300 °C for 10 h in air. The sintered pellets were ground and evaluated by XRD. As shown in Figure 7, trace amounts of impurities were found for $\text{Sr}_2\text{Mg}_{0.3}\text{Ni}_{0.7}\text{MoO}_{6-\delta}$ + LSGM (Figure 7a), while no impurity peaks were detectable for $\text{Sr}_2\text{Mg}_{0.95}\text{Ni}_{0.05}\text{MoO}_{6-\delta}$ + SDC (Figure 7b), indicating that the $\text{Sr}_2\text{Mg}_{0.3}\text{Ni}_{0.7}\text{MoO}_{6-\delta}$ anode material is chemically compatible with SDC below 1300 °C. However, Marrero-López et al.³⁴ found that a minor impurity was observed for SMMO + SDC above 1200 °C. The discrepancy is possibly related to the high synthesis temperature of SMMO powders (1250 °C) in this work, which could lead to lower reactivity of the material.

3.4. Effect of Buffer Layer on Electrochemical Performance. Although Ni-doped SMMO displayed excellent chemical compatibility with the electrolyte SDC, the electronic conduction feature of SDC would reduce the open-circuit voltage (OCV) and therefore the energy efficiency of cells under SOFC operating conditions. In order to obtain a high OCV for the fuel cell, LSGM was used as the electrolyte and SDC was employed as a buffer layer to avert the chemical reaction between LSGM and Ni-doped SMMO. The electrochemical performance of cells with and without the buffer layer was evaluated in an electrolyte-supported configuration with a 400 μm thick LSGM pellet as the electrolyte. Figure 8 presents the E–J curves for $\text{Sr}_2\text{Mg}_{0.7}\text{Ni}_{0.3}\text{MoO}_{6-\delta}$ /LSGM/SmBaCo₂O_{5+δ} and $\text{Sr}_2\text{Mg}_{0.7}\text{Ni}_{0.3}\text{MoO}_{6-\delta}$ /SDC/LSGM/SmBaCo₂O_{5+δ} cells in pure H₂ at 800 °C. The cell with the SDC buffer layer exhibited much better performance than that without the buffer layer. To confirm the effect of buffer layer, the electrochemical impedance spectroscopy (EIS) analysis of symmetrical $\text{Sr}_2\text{Mg}_{0.7}\text{Ni}_{0.3}\text{MoO}_{6-\delta}$ /LSGM/ $\text{Sr}_2\text{Mg}_{0.7}\text{Ni}_{0.3}\text{MoO}_{6-\delta}$ and $\text{Sr}_2\text{Mg}_{0.7}\text{Ni}_{0.3}\text{MoO}_{6-\delta}$ /SDC/LSGM/SDC/ $\text{Sr}_2\text{Mg}_{0.7}\text{Ni}_{0.3}\text{MoO}_{6-\delta}$ cells was performed, and the results are shown in Figure 9. The EIS results for the symmetrical cells with and without the buffer layer revealed that there was no significant change in the LF arc but an obvious decrease in the HF arc when the buffer layer was included, indicating an improved oxygen ion transfer process in the cell with SDC buffer layer. The large HF arc in the cell without the buffer layer should be related to the reactivity between the LSGM electrolyte and the $\text{Sr}_2\text{Mg}_{0.7}\text{Ni}_{0.3}\text{MoO}_{6-\delta}$ anode, which could

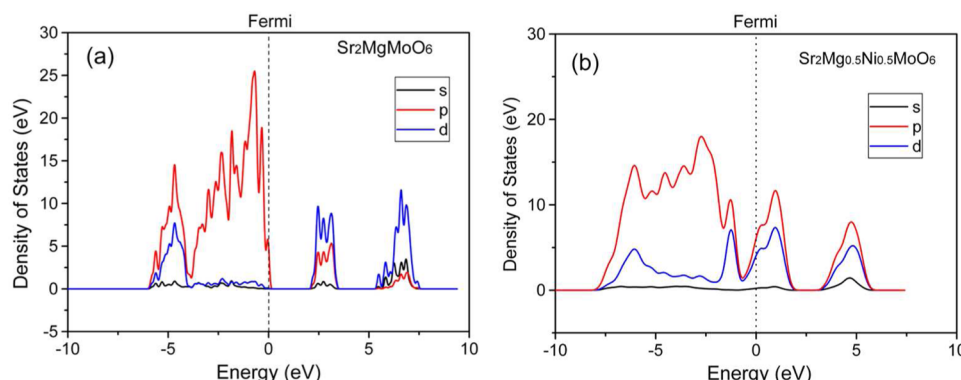


Figure 6. Electronic densities of states of (a) SMMO and (b) $\text{Sr}_2\text{Mg}_{0.5}\text{Ni}_{0.5}\text{MoO}_6$ materials as functions of energy.

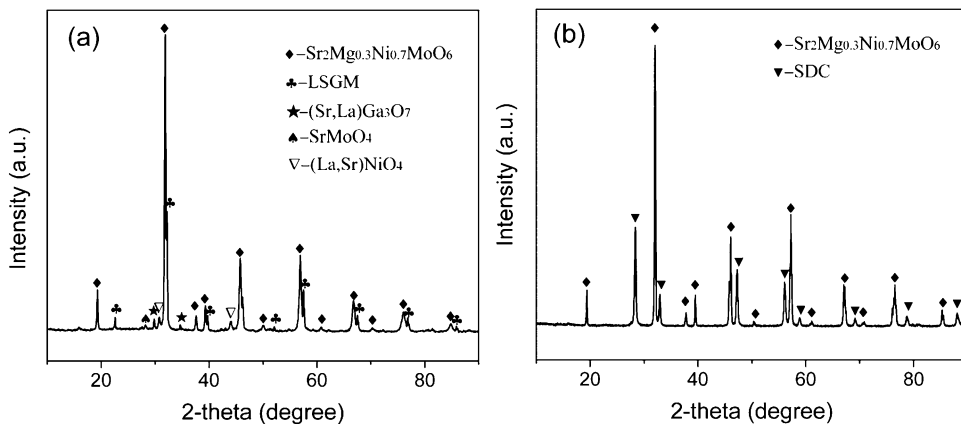


Figure 7. XRD patterns of mixtures of (a) $\text{Sr}_2\text{Mg}_{0.3}\text{Ni}_{0.7}\text{MoO}_6$ and LSGM and (b) $\text{Sr}_2\text{Mg}_{0.3}\text{Ni}_{0.7}\text{MoO}_6$ and SDC after heat treatment at 1300 °C for 10 h in air.

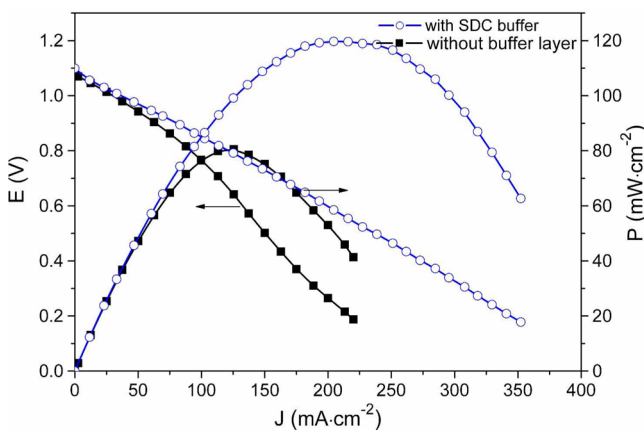


Figure 8. Plots of potential (E) and power density (P) vs current density (J) for cells with and without an SDC buffer layer ($\text{Sr}_2\text{Mg}_{0.7}\text{Ni}_{0.3}\text{MoO}_{6-\delta}/\text{LSGM}/\text{SmBaCo}_2\text{O}_{5+\delta}$ and $\text{Sr}_2\text{Mg}_{0.7}\text{Ni}_{0.3}\text{MoO}_{6-\delta}/\text{SDC}/\text{LSGM}/\text{SmBaCo}_2\text{O}_{5+\delta}$, respectively) at 800 °C in humidified pure hydrogen.

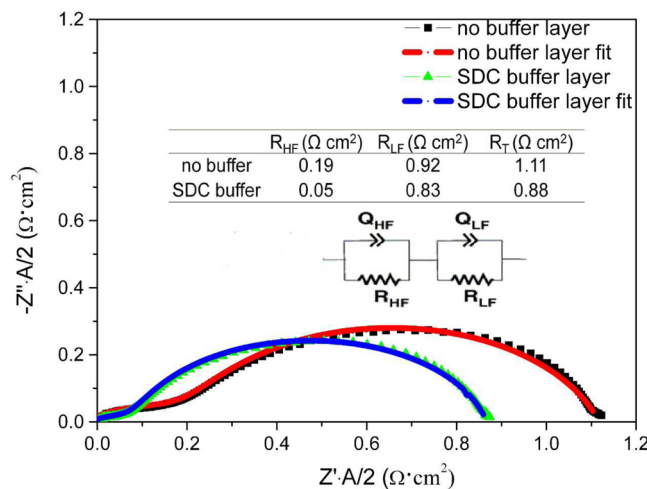


Figure 9. Impedance spectra of symmetrical $\text{Sr}_2\text{Mg}_{0.7}\text{Ni}_{0.3}\text{MoO}_{6-\delta}/\text{LSGM}/\text{Sr}_2\text{Mg}_{0.7}\text{Ni}_{0.3}\text{MoO}_{6-\delta}$ cells with and without an SDC buffer layer measured at 800 °C under 5% H_2/Ar .

lead to the generation of an insulating phase that hinders the oxygen ion transport at the electrode–electrolyte interface and thus decreases the power density of the cell.

3.5. Effect of Ni Content on Electrochemical Performance. AC impedance measurements were performed on a series of symmetrical cells, $\text{Sr}_2\text{Mg}_{1-x}\text{Ni}_x\text{MoO}_{6-\delta}/\text{SDC}/\text{LSGM}/\text{Sr}_2\text{Mg}_{1-x}\text{Ni}_x\text{MoO}_{6-\delta}$ ($x = 0, 0.1, 0.3, 0.5$ and 0.7), at 800 °C under a humidified 5% H_2/Ar atmosphere to gain insight into the role of Ni doping on the polarization resistance of SMNM electrodes. The Nyquist plots and the equivalent circuit used for simulating the electrode reaction process in these symmetrical cells are shown in Figure 10. For the purpose of

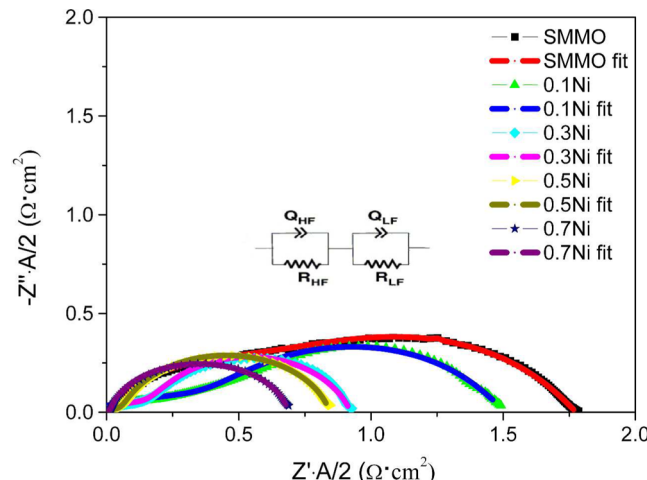


Figure 10. Impedance spectra of symmetrical $\text{Sr}_2\text{Mg}_{1-x}\text{Ni}_x\text{MoO}_{6-\delta}/\text{SDC}/\text{LSGM}/\text{Sr}_2\text{Mg}_{1-x}\text{Ni}_x\text{MoO}_{6-\delta}$ cells recorded under 5% H_2/Ar in the open-circuit state at 800 °C.

determining the effect of Ni doping on the electrode polarization, the ohmic resistances of the symmetrical cells were subtracted from the impedance spectra. The impedance spectra of $\text{Sr}_2\text{Mg}_{0.5}\text{Ni}_{0.5}\text{MoO}_{6-\delta}$ and $\text{Sr}_2\text{Mg}_{0.3}\text{Ni}_{0.7}\text{MoO}_{6-\delta}$ cells showed one dominating semicircle, whereas SMMO, $\text{Sr}_2\text{Mg}_{0.9}\text{Ni}_{0.1}\text{MoO}_{6-\delta}$ and $\text{Sr}_2\text{Mg}_{0.7}\text{Ni}_{0.3}\text{MoO}_{6-\delta}$ cells exhibited two arcs, HF and LF arcs.

As shown in Figure 10, not only the resistance of the total arc (R_t) but also the resistances of the HF arc (R_{HF}) and the LF arc (R_{LF}) exhibited a significantly decreasing tendency with increasing Ni-doping amount in SMNM. For electrodes with high Ni content, the HF arc tended toward being undetectable. The decrease in R_{HF} is most probably due to the improved sinterability of the SMNM anode with increased Ni doping,

which ensures close interfacial contact between electrode/electrolyte and electrode particles, thereby promoting oxygen ion transfer in the electrode. The decrease in R_{LF} suggests that Ni doping in SMMO promotes the catalytic charge transfer and gas adsorption/desorption processes.

To further understand the thermal stability of samples under a reducing atmosphere, H₂ TPR was employed to detect the oxygen release and metal element reduction processes. Figure 11 shows the TPR curves of doped and undoped samples. A

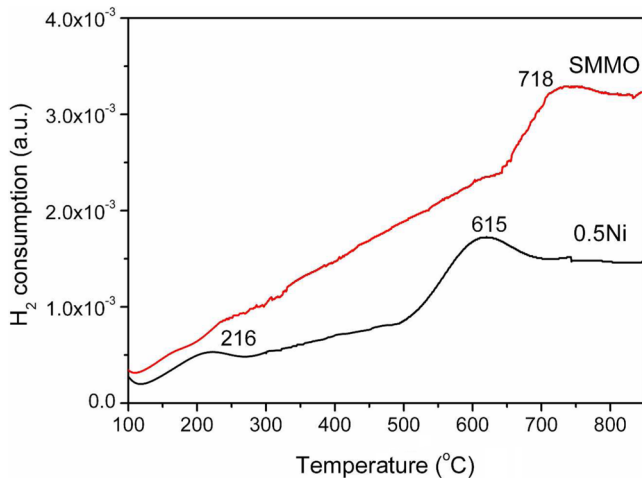


Figure 11. Hydrogen temperature-programmed reduction curves of SMMO (red) and $\text{Sr}_2\text{Mg}_{0.5}\text{Ni}_{0.5}\text{MoO}_{6-\delta}$ (black).

peak near 220 °C was observed for the Ni-doped sample, which should be ascribed to the reduction of adsorbed oxygen.³⁵ The peaks around 610 and 720 °C for SMMO and Ni-doped SMMO are attributed to the reduction of Mo⁶⁺ to Mo⁵⁺.³⁶ The reduction temperature decreased with Ni doping, demonstrating that Ni doping promotes the reduction of surface Mo⁶⁺ to Mo⁵⁺, which is beneficial for the improvement of the catalytic activity of SMMO. This result agrees well with the binding energy calculations and XPS measurements.

The anode performances of the SMMO and $\text{Sr}_{2-x}\text{Ni}_x\text{MoO}_{6-\delta}$ were examined in single cells with an electrolyte-supported configuration using wet H₂ as fuel. Figure 12 presents a cross-sectional image of a typical $\text{Sr}_2\text{Mg}_{0.3}\text{Ni}_{0.7}\text{MoO}_{6-\delta}$ /LSGM/SmBaCo₂O_{5+δ} single cell. The thicknesses of the electrolyte, anode, and cathode layers are ca. 400, 340, and 200 μm, respectively. Figure 13 displays the E-J curves for $\text{Sr}_2\text{Mg}_{1-x}\text{Ni}_x\text{MoO}_{6-\delta}$ ($x = 0, 0.3, 0.7$)/SDC/LSGM/SmBaCo₂O_{5+δ} cells at 800 °C. The Ni doping enhances the power density (P) of the cells, which is mainly related to the increased electronic conductivity and the enhanced catalytic activity of Ni-doped SMMO. The cell with the $\text{Sr}_2\text{Mg}_{0.3}\text{Ni}_{0.7}\text{MoO}_{6-\delta}$ anode delivered a highest power density of 160 mW cm⁻² at 800 °C. In view of the low electrical conductivity of SMMO and the thick electrolyte (400 μm), the power density is acceptable. Further optimization of the microstructure of the electrode and a reduction in the thickness of electrolyte would further improve the cell performance.

4. CONCLUSIONS

Substitution of Ni for Mg in the double perovskite $\text{Sr}_2\text{MgMoO}_{6-\delta}$ yielded new series of $\text{Sr}_2\text{Mg}_{1-x}\text{Ni}_x\text{MoO}_{6-\delta}$ oxides. The solid solution limit of the Ni content (x) in $\text{Sr}_2\text{Mg}_{1-x}\text{Ni}_x\text{MoO}_{6-\delta}$ was $x < 0.9$ for samples sintered at 1450

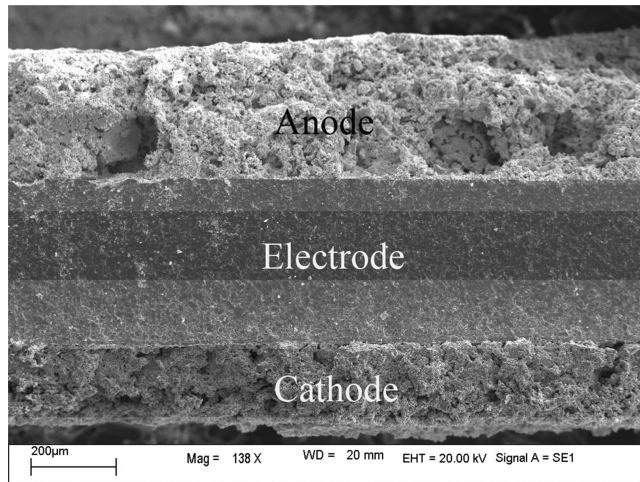


Figure 12. Cross-sectional SEM image of a $\text{Sr}_2\text{Mg}_{0.3}\text{Ni}_{0.7}\text{MoO}_{6-\delta}$ /LSGM/SmBaCo₂O_{5+δ} single cell.

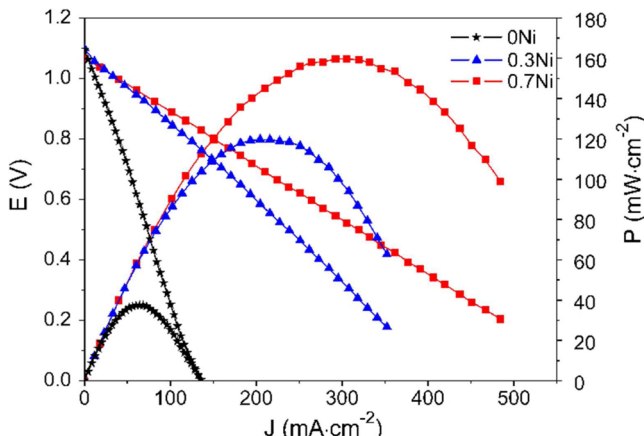


Figure 13. Plots of potential and power density vs current density for cells in the configuration $\text{Sr}_2\text{Mg}_{1-x}\text{Ni}_x\text{MoO}_{6-\delta}$ ($x = 0, 0.3, 0.7$)/SDC/LSGM/SmBaCo₂O_{5+δ} at 800 °C under humidified pure hydrogen.

°C in air and then reduced at 800 °C in 5% H₂/Ar. The $\text{Sr}_2\text{Mg}_{1-x}\text{Ni}_x\text{MoO}_{6-\delta}$ anodes were chemically compatible with SDC electrolyte but slightly reactive with LSGM electrolyte above 1300 °C.

Ni doping increased the electrical conductivity of $\text{Sr}_2\text{Mg}_{1-x}\text{Ni}_x\text{MoO}_{6-\delta}$ as a result of the increased electronic defect concentration [$\text{Mo}_{\text{Mo}^{6+}}^{5+}$] and the decreased band gap energy for electron transport. The electrocatalytic properties of the SMNM anode were sensitive to the current collector, and Pt was not suitable for use as the current collector in SMMO-based cell evaluation. Ni doping significantly facilitated the charge transfer and gas absorption/desorption processes of SMMO and thereby decreased the area-specific resistance of the electrode. The electrode performance of SMMO in single cells was considerably improved with Ni doping, which was related to not only the increased electrical conductivity but also the enhanced electrocatalytic activity. The increased surface-active oxygen, as revealed by TPR and XPS, was indicative of the improved electrocatalytic activity of the SMNO electrode. It is believed that the cell performance could be further improved by optimizing the cell microstructure and reducing the electrolyte thickness. SMNM is a potential anode material for SOFCs.

AUTHOR INFORMATION

Corresponding Author

*Tel: +86-10-82376837. Fax: +86-10-82376837. E-mail: hlzhao@ustb.edu.cn.

Notes

The authors declare no competing financial interest.

ACKNOWLEDGMENTS

This work was kindly supported by the National Basic Research Program of China (2013CB934003), the Guangdong Industry-Academy-Research Alliance (2013CB934003), and the National Natural Science Foundation of China (51302275).

REFERENCES

- (1) Steele, B. C. H.; Heinzel, A. Materials for Fuel-Cell Technologies. *Nature* **2001**, *414*, 345–352.
- (2) Gorte, R. J.; Kim, H.; Vohs, J. M. Novel SOFC Anode for the Direct Electrochemical Oxidation of Hydrocarbon. *J. Power Sources* **2002**, *106*, 10–15.
- (3) Zhu, W. Z.; Deevi, S. C. A Review on the Status of Anode Materials for Solid Oxide Fuel Cells. *Mater. Sci. Eng., A* **2003**, *362*, 228–239.
- (4) Fu, Q. X.; Tietz, F.; Stover, D. La_{0.4}Sr_{0.6}Ti_{1-x}Mn_xO_{3-δ} Perovskites as Anode Materials for Solid Oxide Fuel Cells. *J. Electrochem. Soc.* **2006**, *153*, D74–D83.
- (5) Jiang, S. P.; Chan, S. H. A Review of Anode Materials Development in Solid Oxide Fuel Cells. *J. Mater. Sci.* **2004**, *39*, 4405–4439.
- (6) Ramirez-Cabrera, E.; Atkinson, A.; Chadwick, D. The Influence of Point Defects on the Resistance of Ceria to Carbon Deposition in Hydrocarbon Catalysis. *Solid State Ionics* **2000**, *136*, 825–831.
- (7) Marina, O. A.; Mogensen, M. High-Temperature Conversion of Methane on a Composite Gadolinia-Doped Ceria-Gold Electrode. *Appl. Catal., A* **1999**, *189*, 117–126.
- (8) Tao, S. W.; Irvine, J. T. S. A Redox Stable Efficient Anode for Solid Oxide Fuel Cells. *Nat. Mater.* **2003**, *2*, 320–323.
- (9) Hui, S.; Petric, A. Evaluation of Yttrium-Doped SrTiO₃ as an Anode for Solid Oxide Fuel Cells. *J. Eur. Ceram. Soc.* **2002**, *22*, 1673–1681.
- (10) Kaiser, A.; Bradley, J. L.; Slater, P. R.; Irvine, J. T. S. Tetragonal Tungsten Bronze Type Phases (Sr_{1-x}Ba_x)_{0.6}Ti_{0.2}Nb_{0.8}O_{3-δ}: Material Characterisation and Performance as SOFC Anodes. *Solid State Ionics* **2000**, *135*, 519–524.
- (11) Holtappels, P.; Poulsen, F. W.; Mogensen, M. Electrical Conductivities and Chemical Stabilities of Mixed Conducting Pyrochlores for SOFC Applications. *Solid State Ionics* **2000**, *135*, 675–679.
- (12) Goodenough, J. B.; Huang, Y. H. Alternative Anode Materials for Solid Oxide Fuel Cells. *J. Power Sources* **2007**, *173*, 1–10.
- (13) Huang, Y. H.; Dass, R. I.; Xing, Z. L.; Goodenough, J. B. Double Perovskites as Anode Materials for Solid-Oxide Fuel Cells. *Science* **2006**, *312*, 254–257.
- (14) Huang, Y. H.; Dass, R. I.; Denysyn, J. C.; Goodenough, J. B. Synthesis and Characterization of Sr₂MgMoO_{6-δ}: An Anode Material for the Solid Oxide Fuel Cell. *J. Electrochem. Soc.* **2006**, *153*, A1266–A1272.
- (15) Bi, Z. H.; Zhu, J. H. Effect of Current Collecting Materials on the Performance of the Double-Perovskite Sr₂MgMoO_{6-δ} Anode. *J. Electrochem. Soc.* **2011**, *158*, B605–B613.
- (16) Howell, T. G.; Kuhnelli, C. P.; Reitz, T. L.; Sukeshini, A. M.; Singh, R. N. A₂MgMoO₆ (A = Sr, Ba) for Use as Sulfur Tolerant Anodes. *J. Power Sources* **2013**, *231*, 279–284.
- (17) Ji, Y.; Huang, Y. H.; Ying, J. R.; Goodenough, J. B. Electrochemical Performance of La-Doped Sr₂MgMoO_{6-δ} in Natural Gas. *Electrochem. Commun.* **2007**, *9*, 1881–1885.
- (18) Marrero-López, D.; Peña-Martínez, J.; Ruiz-Morales, J. C.; Martín-Sedeño, M. C.; Núñez, P. High Temperature Phase Transition in SOFC Anodes Based on Sr₂MgMoO_{6-δ}. *J. Solid State Chem.* **2009**, *182*, 1027–1034.
- (19) Zhang, L. L.; He, T. M. Performance of Double-Perovskite Sr_{2-x}Sm_xMgMoO_{6-δ} as Solid Oxide Fuel Cell Anodes. *J. Power Sources* **2011**, *196*, 8352–8359.
- (20) Vasala, S.; Lehtimäki, M.; Haw, S. C.; Chen, J. M.; Liu, R. S.; Yamauchi, H.; Karppinen, M. Isovalent and Aliovalent Substitution Effects on Redox Chemistry of Sr₂MgMoO_{6-δ} SOFC-Anode Material. *Solid State Ionics* **2010**, *181*, 754–759.
- (21) Escudero, M. J.; Gómez de Parade, I.; Fuerte, A.; Daza, L. Study of Sr₂Mg(Mo_{0.8}Nb_{0.2})O_{6-δ} as Anode Material for Solid Oxide Fuel Cells Using Hydrocarbons as Fuel. *J. Power Sources* **2013**, *243*, 654–660.
- (22) Bernuy-Lopez, C.; Allix, M.; Bridges, C. A.; Claridge, J. B.; Rosseinsky, M. J. Sr₂MgMoO_{6-δ}: Structure, Phase Stability, and Cation Site Order Control of Reduction. *Chem. Mater.* **2007**, *19*, 1035–1043.
- (23) Matsuda, Y.; Karppinen, M.; Yamazaki, Y.; Yamauchi, H. Oxygen-Vacancy Concentration in Sr₂MgMoO_{6-δ} Double-Perovskite Oxides. *J. Solid State Chem.* **2009**, *182*, 1713–1716.
- (24) Xie, Z.; Zhao, H.; Du, Z.; Chen, T.; Chen, N.; Liu, X.; Skinner, S. J. Effects of Co Doping on the Electrochemical Performance of Double Perovskite Oxide Sr₂MgMoO_{6-δ} as an Anode Material for Solid Oxide Fuel Cells. *J. Phys. Chem. C* **2012**, *116*, 9734–9743.
- (25) Huang, Y. H.; Liang, G.; Croft, M.; Lehtimäki, M.; Karppinen, M.; Goodenough, J. B. Double-Perovskite Anode Materials Sr₂MMoO₆ (M = Co, Ni) for Solid Oxide Fuel Cells. *Chem. Mater.* **2009**, *21*, 2319–2326.
- (26) Zhang, P.; Huang, Y. H.; Cheng, J. G.; Mao, Z. Q.; Goodenough, J. B. Sr₂CoMoO₆ Anode for Solid Oxide Fuel Cell Running on H₂ and CH₄ Fuels. *J. Power Sources* **2011**, *196*, 1738–1743.
- (27) Hung, K. Q.; Goodenough, J. B. Wet Chemical Synthesis of Sr- and Mg-Doped LaGaO₃, a Perovskite-Type Oxide-Ion Conductor. *J. Solid State Chem.* **1998**, *136*, 274–283.
- (28) Xie, Z.; Zhao, H.; Chen, T.; Zhou, X.; Du, Z. Synthesis and Electrical Properties of Al-Doped Sr₂MgMoO_{6-δ} as an Anode Material for Solid Oxide Fuel Cells. *Int. J. Hydrogen Energy* **2011**, *36*, 7257–7264.
- (29) Perdew, J. P.; Burke, K.; Ernzerhof, M. Generalized Gradient Approximation Made Simple. *Phys. Rev. Lett.* **1996**, *77*, 3865–3868.
- (30) Vasala, S.; Lehtimäki, M.; Huang, Y. H.; Yamauchi, H.; Goodenough, J. B.; Karppinen, M. Degree of Order and Redox Balance in B-Site Ordered Double-Perovskite Oxides, Sr₂MMoO_{6-δ} (M = Mg, Mn, Fe, Co, Ni, Zn). *J. Solid State Chem.* **2010**, *183*, 1007–1012.
- (31) Kim, D.; Kagwade, S. V.; Clayton, C. R. Identification of Mo(V) Commonly Observed in Passive Films Formed on Stainless Steels. *Surf. Interface Anal.* **1998**, *26*, 155–159.
- (32) Dambies, L.; Guimon, C.; Yiakoumi, S.; Guibal, E. Characterization of Metal Ion Interactions with Chitosan by X-ray Photoelectron Spectroscopy. *Colloids Surf., A* **2000**, *177*, 203–214.
- (33) Marrero-López, D.; Peña-Martínez, J.; Ruiz-Morales, J. C.; Pérez-Coll, D.; Aranda, M. A. G.; Núñez, P. Synthesis, Phase Stability and Electrical Conductivity of Sr₂MgMoO_{6-δ} Anode. *Mater. Res. Bull.* **2008**, *43*, 2441–2450.
- (34) Marrero-López, D.; Peña-Martínez, J.; Ruiz-Morales, J. C.; Gabás, M.; Núñez, P.; Aranda, M. A. G.; Ramos-Barrado, J. R. Redox Behaviour, Chemical Compatibility and Electrochemical Performance of Sr₂MgMoO_{6-δ} as SOFC Anode. *Solid State Ionics* **2010**, *180*, 1672–1682.
- (35) Yin, Y. M.; Xiong, M. W.; Yang, N. T.; Tong, Z.; Guo, Y. Q.; Ma, Z. F.; Sun, E.; Yamanis, J.; Jing, B. Y. Investigation on Thermal, Electrical, and Electrochemical Properties of Scandium-Doped Pr_{0.6}Sr_{0.4}(Co_{0.2}Fe_{0.8})_{1-x}Sc_xO_{3-δ} as Cathode for IT-SOFC. *Int. J. Hydrogen Energy* **2011**, *36*, 3989–3996.
- (36) Arnoldy, P.; De Jonge, J. C. M.; Moulijn, J. A. Temperature-Programmed Reduction of Molybdenum(VI) Oxide and Molybdenum(IV) Oxide. *J. Phys. Chem.* **1985**, *89*, 4517–4526.